Mesoscale Eddies in the South China Sea

5

Hongyang Lin* and Zhenyu Sun

State Key Laboratory of Marine Environmental Science, College of Ocean and Earth Sciences, Xiamen University, Xiamen, Fujian, China
*hylin@xmu.edu.cn

Mesoscale eddies are ubiquitous in the South China Sea (SCS) and play an important role in local thermodynamics and biogeochemistry. This chapter reviews the (i) horizontal statistical features, (ii) vertical structures and (iii) dynamical impacts of mesoscale eddies in the SCS. Eddies are generated almost everywhere in the SCS deep basin with key regions in the southwest of Taiwan, west of Luzon and southeast of Vietnam. Eddy properties such as lifespan, size and propagation are generally in qualitative agreement among existing studies, whereas eddy numbers differ considerably due to different identification methods and criteria. Vertical structures of eddies in the SCS are overviewed through several prominent examples. While the majority of eddies are surface-intensified, they have prominent influences in the interior. Observational studies reported the interesting southwestward tilt of vertical axis of eddy centers, of which the mechanism is still unclear. Environmental responses to eddies are reviewed by examining eddy-induced changes in thermohaline properties and circulation, heat and salt transports, air–sea interactions and biogeochemical tracers. Future orientations are also discussed including possible roles of submesoscale processes in advancing the current understanding of mesoscale dynamics and energetics.

5.1 Introduction

Oceanic mesoscale processes, typically with spatial scales of tens to hundreds of kilometers and temporal scales of tens to hundreds of days, are

primarily in geostrophic balance carrying the largest part of oceanic kinetic energy [Ferrari and Wunsch, 2009]. Such mesoscale phenomena occur in the ocean as Rossby waves, eddies (also termed as vortices), meanders, etc. Mesoscale eddies have been found to be ubiquitous in the global ocean [Chelton *et al*., 2007b, 2011]. Some strong, coherent eddies are also called as rings, which are often pinched off from strong currents and observed in their extensions. In contrast to linear Rossby waves, most eddies are strongly nonlinear, suggesting their distinguishing roles in the transport of, for example, heat, salt and momentum.

In the global ocean, investigation of mesoscale eddies was initiated in the Gulf Stream [Iselin and Fuglister, 1948]. In the South China Sea (SCS), the earliest discovery of mesoscale eddies was made by Dale [1956]. Since then, however, investigations of mesoscale eddies in the SCS have still been sparse and intermittent due to very limited observations. The advent of satellite altimetry provides an unprecedented opportunity to study oceanographic mesoscale phenomena, and thus mesoscale eddy study in the SCS has become a hot spot over the past two decades.

In the pre-altimetry era, mesoscale eddies had also been documented in the SCS based on *in situ* measurements. For example, based on an analysis of 50 years (1921–1970) of historical hydrographic measurements, Xu *et al.* [1982] observed multiple "mesoscale circulation" structures embedded in the basin-scale circulation from maps of the calculated geostrophic currents (Figure 5.1). These early-stage reports were crucial in advancing the understanding of SCS multiscale circulations and dynamics at that time. In the early years of post-altimetry era, *in situ* measurements were still important means to study mesoscale eddies in the SCS [e.g., Wang and Chern, 1987a, 1987b, 1997; Li *et al*., 1998]. Nevertheless, *in situ* measurements have been scarce over the past few decades due to high cost, and hence have been inadequate to gain the overall characteristics of mesoscale eddies in the SCS.

In this chapter, we will focus on studies on mesoscale eddies in the SCS in the post-altimetry period with integrated data sources. Many studies mentioned here use a combination of multiple satellite observations, *in situ* measurements and numerical simulations. Recently, Zheng *et al.* [2017] provided an overview on the progress in mesoscale eddy studies in the SCS, and grouped them into three stages of studies: (i) early discoveries, and eddies being treated as (ii) a single water mass motion and (iii) grouped water mass motion. They briefly reviewed the common

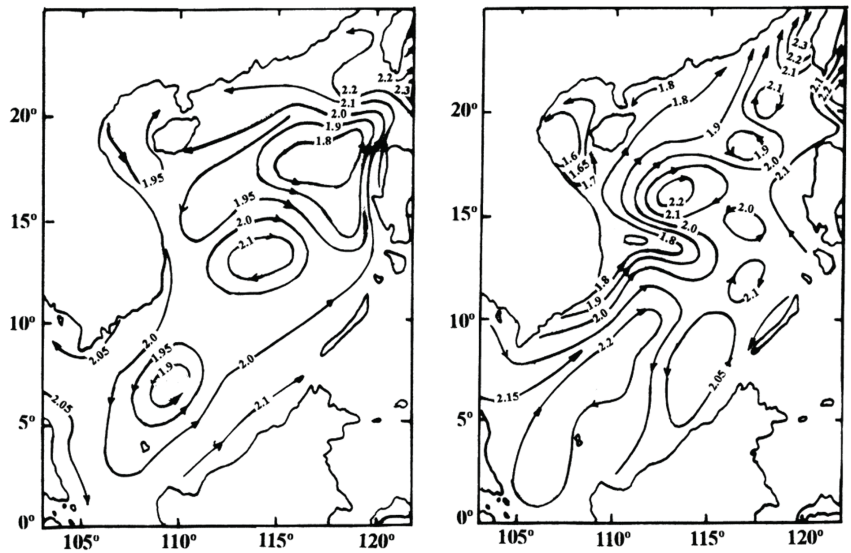

Fig. 5.1. Surface geostrophic currents in (a) winter and (b) summer, calculated based on historical hydrographic measurements in the SCS.

Source: Redrawn from Xu *et al.* [1982].

results of eddy properties and structures, and discussed more about the mechanisms/sources of the SCS eddies. This chapter, on the other hand, shows detailed statistical results including eddy detection methods, summarizes the horizontal distribution and vertical structure of mesoscale eddies and concentrates more on impacts of eddies on the physical and biogeochemical environments in the SCS. Therefore, this chapter could be treated as a companion of Zheng *et al.* [2017] in terms of providing a more comprehensive review of mesoscale eddy studies in the SCS.

This chapter is structured as follows: Section 5.2 summarizes the horizontal features of mesoscale eddies in the SCS, including the spatial distribution, statistical eddy properties and their time variations. Section 5.3 provides the vertical structure of mesoscale eddies in the SCS through several prominent examples. Section 5.4 focuses on the influences of mesoscale eddies on the local thermohaline structure and circulation, turbulent mixing, atmosphere and biogeochemical processes. A summary is given in Section 5.5.

5.2 Horizontal Distribution and Statistical Properties of Mesoscale Eddies in the SCS

5.2.1 *Spatial distribution of mesoscale eddies*

Systematical detection of mesoscale eddies in the SCS was initiated at the beginning of this century. Overall, mesoscale eddies appear to occur in most places of the SCS deep basin. Several regions have been identified to be key areas in terms of vigorous eddy activities (e.g., southwest of Taiwan, southeast of the Vietnam coast, west of Luzon, etc.) as detailed in what follows. These regions generally coincide with areas having high eddy kinetic energy [Chen *et al*., 2009; Cheng and Qi, 2010].

Using 5.6 years (from December 1992 to August 1998) of TOPEX/Poseidon altimeter data, Hwang and Chen [2000] identified eddies in the SCS from contour maps of sea surface height (SSH). Focusing on eddies with lifetimes longer than a month and with radii larger than 150 km, they found that both anticyclonic and cyclonic eddies occurred almost everywhere in the SCS with hotspots east of Vietnam, west of Luzon and east of the Xisha Islands, forming a northeast–southwest band across the SCS basin.

Using eight years (1993–2000) of merged gridded altimeter data, Wang *et al.* [2003] detected mesoscale eddies in the SCS according to a set of criteria: (i) closed sea level contours, (ii) the water depth of eddy center deeper than 1000 m, (iii) eddy amplitude (sea level difference between eddy center and boundary) greater than 7.5 cm, (iv) eddy lifetime longer than 30 days, and (v) if the above four criteria are satisfied, the eddy can be traced back in time given eddy amplitude greater than 4 cm. The identified eddies over the eight-year period were grouped into four geographic zones (Figure 5.2): eddies generated in the southwest of Taiwan (Zone 1) were believed to be associated with the Kuroshio intrusion and frontal instabilities, northwest of Luzon (Zone 2) associated with the wind stress curl or vorticity advection from the Kuroshio front, southwest of Luzon (Zone 3) possibly associated with shelf current-topography interactions, and offshore of Central Vietnam (Zone 4) associated with the eastward baroclinic jet.

After the pioneering works of Hwang and Chen [2000] and Wang *et al.* [2003], there have been many successive studies on mesoscale eddies in the SCS based on altimeter data or numerical simulations. For example, Cheng *et al.* [2005], Lin *et al.* [2007], and Chen *et al.* [2011] investigated the spatiotemporal variability of mesoscale eddies in the SCS using merged

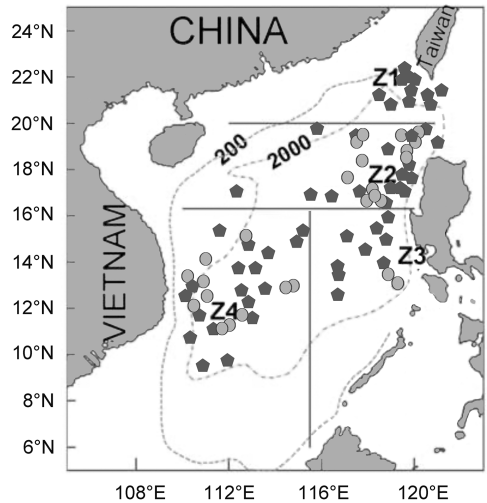

Fig. 5.2. Distribution of mesoscale eddies in the SCS identified over the years 1993–2000. Cyclonic and anticyclonic eddies are marked with solid circles and dark pentagons, respectively.

Source: Redrawn from Wang *et al.* [2003].

altimeter data from longer periods. Xiu *et al.* [2010] and Lin *et al.* [2015] examined the SCS eddy activities based on 3D primitive equation numerical simulations. Different eddy identification schemes have been used in the previously mentioned studies, including the SSH-based method [Cheng *et al*., 2005; Lin *et al*., 2007] as implemented by Wang *et al.* [2003], the winding angle method [Sadarjoen and Post, 2000; Chaigneau *et al.* 2008; Chen *et al*., 2011], the Okubo–Weiss method [Okubo, 1970; Weiss, 1991; Xiu *et al*., 2010], and the vector geometry-based method [Nencioli *et al*., 2010; Lin *et al*., 2015]. In general, the overall patterns of geographic distribution of mesoscale eddies in the SCS are similar among these studies, although the specific properties (e.g., annual mean number, eddy amplitude, etc.) are different to a certain degree, as expected from the different data sources, processing procedures, eddy identification methods and criteria being used.

5.2.2 *Statistical features of eddy properties*

Given the numerous studies on mesoscale eddies in the SCS mentioned previously, a number of statistical characteristics of eddy properties could

be summarized. Typically, previous investigators focused on properties like eddy number, lifetime, radius, propagation features and so on. Although many studies provide certain aspects of the properties, the reader is referred to Chen *et al.* [2011] for a comprehensive summary of the statistical properties of mesoscale eddies in the SCS.

***Eddy number*:** There are considerable discrepancies in the detected annual eddy numbers in the SCS among existing studies. Wang *et al.* [2003] identified 58 anticyclonic and 28 cyclonic eddies over the period 1993–2000, giving an average of 10.8 eddies per year. By contrast, the detected annual mean eddy number was 18.1 in Lin *et al.* [2007], 32.8 ± 3.4 based on altimetry and 32.9 ± 2.4 based on model output in Xiu *et al.* [2010], 48.6 in Chen *et al.* [2011], 21.5 ± 4 in Lin *et al.* [2012] and even 130.5 based on altimetry and 123.9 based on model output in Lin *et al.* [2015]. One can see relatively large differences in the detected eddy numbers among these studies, and the primary cause is the different criteria and eddy detection algorithms used. In this sense, it is difficult to reach a consensus on a widely accepted annual eddy number in the SCS.

***Eddy lifetime*:** Lin *et al.* [2007] indicated that almost all detected eddies had a lifespan less than 180 d and those between 30 d and 60 d occupied the largest proportion. Based on model output, Xiu *et al.* [2010] found 53% of simulated eddies had a lifetime shorter than 60d. Chen *et al.* [2011] estimated that the averaged lifetime for an eddy was 8.8 weeks (62 d), and 74% of the detected eddies had a lifespan shorter than 10 weeks. Lin *et al.* [2015] suggested that 70% of the simulated eddies in the upper 700 m had a lifespan shorter than 60 d. In general, decreasing eddy numbers are associated with increasing eddy lifetimes, though exceptions exist. Chen *et al.* [2011] also showed that smaller-sized eddies tended to have shorter lifetimes and stronger intensities.

***Eddy radius*:** By excluding eddies with radii smaller than 50 km, Lin *et al.* [2007] found most eddies had a radius of 100–250 km, with 200 km being most likely. Xiu *et al.* [2010] showed that the radius for simulated eddies ranged from 46.5 to 223.5 km, with an average of 87.4 km. Based on altimeter data, Chen *et al.* [2011] suggested that 64% of the total detected eddies had a radius of 100–200 km with 130 km possessing the highest probability. The model output of Lin *et al.* [2015] indicated that eddies with a radius of 20–30 km corresponded to the largest eddy numbers, and the averaged eddy radius decreased from 50 km at sea surface to 40 km at 700 m. Both

Lin *et al.* [2007] and Chen *et al.* [2011] linked the eddy radius in the SCS to the local Rossby radius of deformation although considerable discrepancies were readily discernible. We note that the estimated eddy radius also depends on the eddy detection method being used. Typical SSH-based methods [e.g., Wang *et al*., 2003; Lin *et al*., 2007] define the eddy boundary as the outermost closed SSH contour encompassing the eddy center, whereas the vector geometry-based method [Lin *et al*., 2015] defines the eddy boundary as the outermost closed streamline which is normally smaller than the SSH-based boundary. One should keep this in mind when comparing statistical eddy radii among different studies.

***Eddy propagation*:** By tracking the eddy trajectories, Lin *et al.* [2007] indicated that over 80% of all detected eddies propagated westward. In the northern SCS, eddies east of 118°E (near Luzon) propagated northwestward, whereas eddies west of 118°E propagated southwestward roughly along the 200 m isobath. In the southern SCS, eddies propagated westward and then turned southward along the 200 m isobath after hitting the western boundary. The predominant westward propagation tendency has also been confirmed by the subsequent studies based on altimeter data [Chen *et al*., 2011] or model output [Xiu *et al*., 2010; Lin *et al*., 2015]. Xiu *et al.* [2010] also noted that slightly more cyclonic (anticyclonic) eddies are deflected equatorward (poleward) based on their model output, which was not consistent with previous findings based on global statistics using satellite altimetry [Morrow *et al*., 2004; Chelton *et al*., 2007b]. With respect to the propagation speed, Lin *et al.* [2007] estimated that it ranges from -8 to $3\,\mathrm{cm\,s^{-1}}$ (minus means westward) with $-2\,\mathrm{cm\,s^{-1}}$ corresponding to the largest probability. They are also reported on a "Σ" shape distribution in the latitude-zonal propagation speed diagram, which was also found by Lin *et al.* [2015] based on their numerical simulations. In particular, Chen *et al.* [2011] derived a climatological vector field of eddy propagation velocity in the $1^\circ \times 1^\circ$ grid (Figure 5.3), which vividly showed the characteristics of eddy propagation in the SCS. The overall propagating features were generally in agreement with the descriptions given in Lin *et al.* [2007].

5.2.3 *Temporal variability of eddy properties*

Compared to statistics on the mean eddy properties, less works focus on the temporal variability of eddy properties in the SCS. Among the

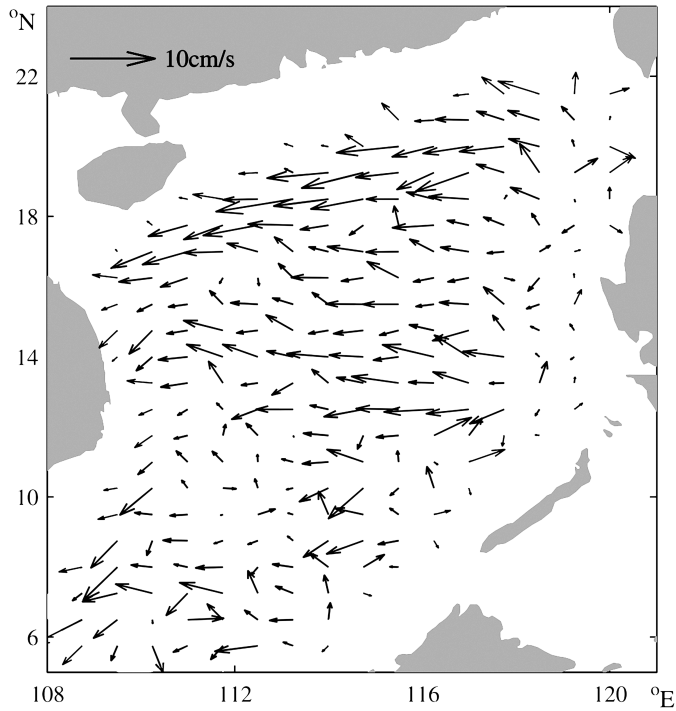

Fig. 5.3. Gridded climatological field of eddy propagation velocity vectors (arrows) for the period from October 1992 to October 2009.

Source: Redrawn from Chen *et al.* [2011].

existing studies on the time-varying eddy properties in the SCS, most of them concentrate on temporal variations in eddy numbers. For example, based on merged satellite altimeter and scatterometer data, Cheng *et al.* [2005] revealed robust seasonal and interannual variabilities of mesoscale eddies in the SCS, and demonstrated that changes in the monsoon winds were likely a key factor in modulating the above temporal variations. The prominent seasonal and interannual variations had also been reported by Lin *et al.* [2012] through monthly and yearly statistics of eddy numbers. They linked the high eddy genesis areas to regions with high eddy kinetic energy and high root-mean-square values of sea level and relative vorticity.

The other hotspot is whether the occurrence of mesoscale eddies in the SCS has potential relationship with El Niño/Southern Oscillation (ENSO)

events. Focusing on eddies with radii larger than 150 km, Hwang and Chen [2000] claimed that the interannual variability of monthly eddy number was linked to ENSO, possibly via ENSO-modulated monsoon winds. Lin *et al.* [2007] held a similar viewpoint based on several coincidences between eddy number and typical El Niño and La Niña years. Nevertheless, solid connections between eddy number and ENSO events had been rarely, if ever, confirmed by subsequent studies. Xiu *et al.* [2010] and Chen *et al.* [2011] directly pointed out that no correspondence had been observed between ENSO events and eddy activities in the SCS. Similar conclusion was also drawn by Zheng *et al.* [2017] in an interpretation of the yearly eddy number distribution from Lin *et al.* [2012]. Recently, Tuo *et al.* [2019] found that the correlation between ENSO and the activity of mesoscale oceanic eddies in the SCS changed around 2004. The mesoscale eddy number was significantly and negatively correlated with the Niño3.4 index before 2004, but the correlation weakened and became insignificant afterward. Further analyses revealed that the ENSO–eddy relation is controlled by two major wind stress forcing mechanisms: one directly related to ENSO and the other indirectly related to ENSO through its subtropical precursor — the Pacific Meridional Mode (PMM).

Another phenomenon related to temporal variation is the intermittent (normally seasonal) recurrence of certain prominent mesoscale eddies in the SCS. The first example is the Luzon Cold Eddy (LCE), which is situated to the northwest of Luzon Island from late fall to early spring [Qu, 2000]. Different mechanisms have been proposed for its generation, including for example the local wind stress curl [Qu, 2000] and forced Rossby waves [Yang and Liu, 2003]. Based on output from a primitive-equation numerical model, Wang and Gan [2014] indicated that although the LCE was generated by the imparted vorticity from the local wind, its asymmetric structure was primarily due to a coexisting anticyclonic eddy to the south. The second example is the eddy pair to the southeast of Vietnam, which, normally occurring in summer, is one prominent feature of the summertime SCS circulation. Based on satellite observations and a reduced gravity model, Wang *et al.* [2006] attributed the formation of this eddy pair (termed as eddy dipole in their paper) to vorticity transports via the western boundary currents associated with a double gyre circulation, which was believed to be generated by a corresponding dipole of local wind stress curl. Chu *et al.* [2017] further pointed out that the occurrence of the eddy pair was linked to the ENSO events, i.e., the eddy pair would disappear in

the summer of a La Niña year if the preceding El Niño event was strong enough.

5.3 Vertical Structures of Mesoscale Eddies in the SCS

This section describes the vertical features of mesoscale eddies in the SCS. This will be achieved by examining several examples of prominent eddies/eddy pairs in an attempt to obtain the generalized 3D features.

5.3.1 *Summertime cold eddy off Vietnam*

Based on a combination of *in situ* measurements and satellite observations, Hu *et al.* [2011] reported the 3D structure of a cyclonic cold eddy off central Vietnam. The cold eddy was part of the eddy pair straddling an eastward coastal baroclinic jet [Gan and Qu, 2008] separated from the southern Vietnam coast. According to satellite altimeter images, the cold eddy persisted for two weeks from late August to mid-September with swift formation and decaying stages (both within 2 days). The observed eddy was heterogeneous in terms of the horizontal and vertical properties according to the measurements from the conductivity–temperature–depth (CTD) profiler and acoustic Doppler current profiler (ADCP). Stronger horizontal currents were observed at the southeastern part of the eddy at each layer associated with the neighboring front to the south. Asymmetries were also seen in the distributions of vorticity and vertical velocity derived using the quasi-geostrophic Omega equation (Figure 5.4). In contrast to traditional expectations, the cyclonic cold eddy experienced both upward and downward motions within the core. The authors attributed the heterogeneity in the vertical velocities to the ageostrophic motions; however, we note that considerable errors are expected in the diagnosis of vertical velocities given the relatively coarse resolution in the *in situ* measurements (0.5° both in zonal and meridional directions). The cold eddy was found to be surface-intensified and the intensity decreased dramatically within the pycnocline, with the vertical axis of eddy center tilted southwestward with increasing depth.

Although a great deal of detailed structures and the underlying dynamics were still unclear at that point, this study was a pioneering observed

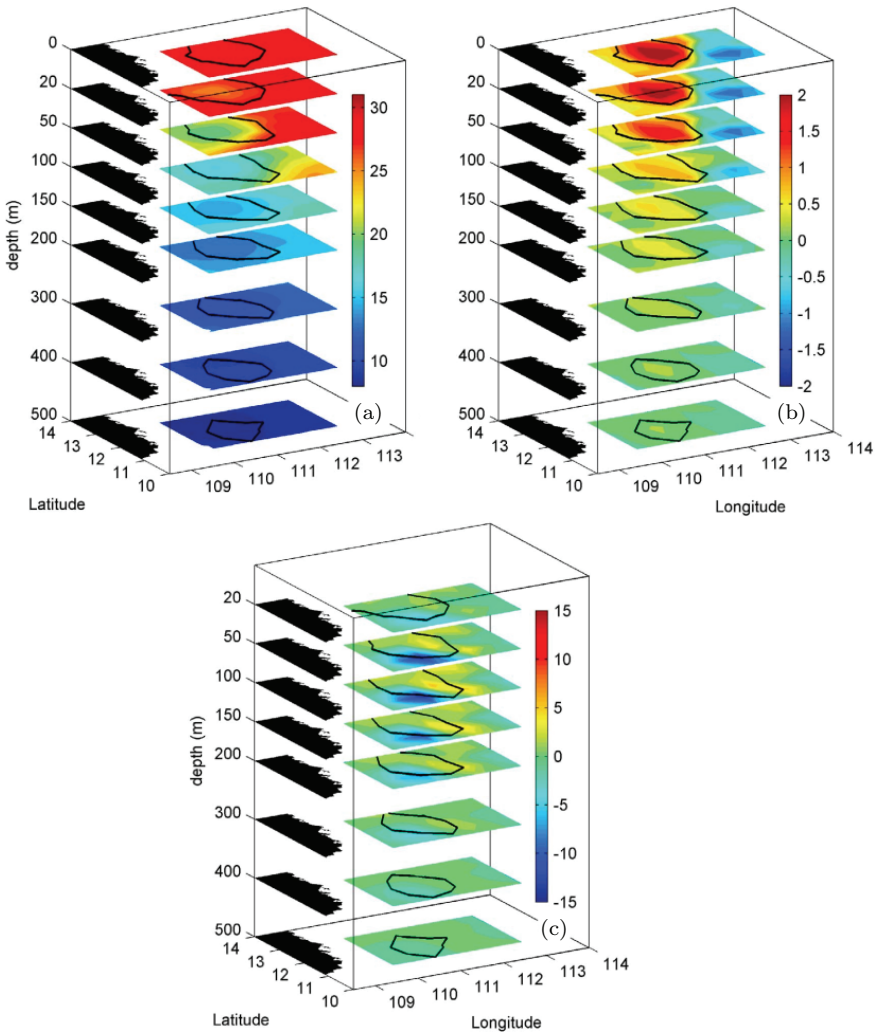

Fig. 5.4. 3D structures of (a) temperature (° C), (b) vorticity (10^{-5} s^{-1}) and (c) vertical velocity (10^{-5} m s^{-1}, positive upward). The black lines are the $-0.2\,\sigma_w$ contours defining the eddy at each depth.

Source: Taken from Hu *et al.* [2011].

documentation of the 3D structure of mesoscale eddies in the SCS. It provided vivid pictures of the vertical structure of a typical eddy and significantly improved our comprehensive understanding of the eddy evolution and dynamics.

5.3.2 *Eddy pair off southwestern Taiwan*

As previously mentioned, southwest of Taiwan is an area associated with high eddy kinetic energy [Wang *et al*., 2003]. Based on 17-year (1992–2009) altimeter data, Nan *et al.* [2011a] found frequent concurrence of anticyclonic and cyclonic eddies (i.e., eddy pair) in this region. Cyclones are more than anticyclones in quantity but the latter often have stronger intensity and longer lifetime. Using three bottom-mounted moorings to the west of Luzon Strait, Zhang *et al.* [2013] investigated the influence of the eddy pair on regional deep circulation and found that the magnitude of deep currents got intensified by a factor of two under the presence of the eddy pair. The surface and deep currents had reversed directions during the eddy event, which was explained with the first baroclinic mode. Their energy analysis based on HYCOM (Hybrid Coordinate Ocean Model) reanalysis data also suggested that both barotropic and baroclinic instabilities played important roles in the generation and growth of the eddy pair.

As a step forward, Zhang *et al.* [2016] used many more mooring arrays (a total of 17 moorings) covering almost the full water column, aiming to gain a more comprehensive understanding of the 3D structure of the eddy pair and the mechanisms controlling its generation and dissipation. The anticyclonic eddy was believed to have been shed from the Kuroshio loop current while the cyclonic eddy was suspected to have originated from the coastal region due to vortex stretching associated with the offshore transport induced by the anticyclonic eddy on its northeastern part. The authors constructed the 3D structure of the eddies using a combination of mooring and altimeter data as well as a particular projection method in a new coordinate system (Figure 5.5). Signals on deep velocities due to the eddy pair were discernible as found in Zhang *et al.* [2013]. Interestingly, the authors also found that the vertical axis of eddies tilts southwestward with increasing depth (Figure 5.5), similar to the documentation in Hu *et al.* [2011], although Zhang *et al.* [2016] claimed that the tilting distance could reach 150 km from sea surface to 1500 m. The other core conclusion of

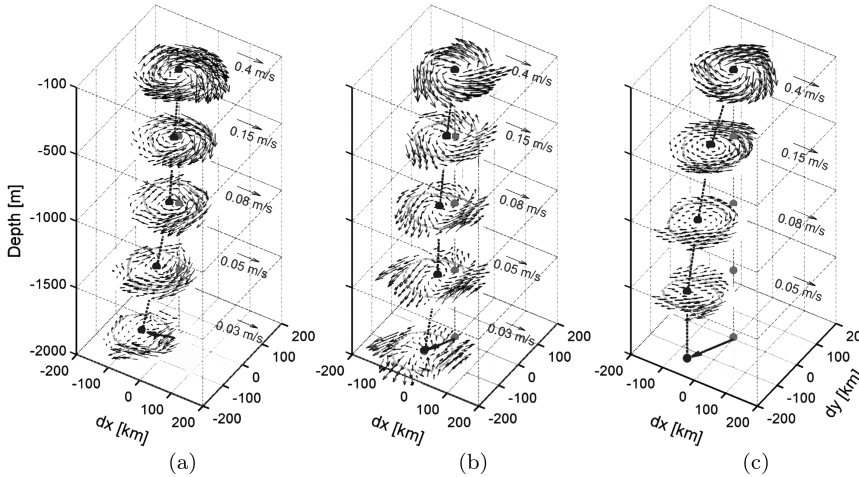

Fig. 5.5. 3D structure of the mesoscale eddies southwest of Taiwan. Velocity vectors are shown by black arrows. Eddy centers at each layer are shown by dots. Dotted line denotes the vertical eddy axis and the thick arrows denote the excursion of eddy center about *z*-axis.

Source: Redrawn from Zhang *et al.* [2016].

Zhang *et al.* [2016] is that the generation of submesoscale motions fed by the mesoscale eddies was the most important factor in the dissipation of the eddy pair, according to their energy budget analysis using available observations.

5.3.3 *Generalized 3D features*

Based on nine-year (2000–2008) output from an eddy-resolving ($1/12^\circ \times 1/12^\circ$) numerical simulation, Lin *et al.* [2015] generated a 3D eddy dataset in the SCS by applying a 3D eddy detection scheme. Specifically, the authors detected eddies at each layer using the eddy detection algorithm of Nencioli *et al.* [2010], then started from the sea surface and moved downward to search to what depth each eddy could penetrate based on the eddy's polarity, radius, etc. A similar searching algorithm had been used in Dong *et al.* [2012]. Their simulations suggested that most eddies were confined to the upper 200 m.

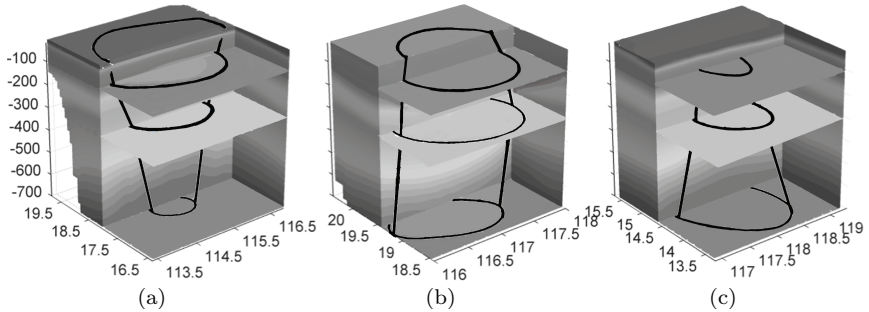

Fig. 5.6. Three types of eddies in terms of vertical structures: (a) bowl-shaped, (b) lens-shaped and (c) cone-shaped. Black contours denote eddy boundaries.

Source: Redrawn from Lin *et al.* [2015].

Based on the depth-varying eddy radius, Lin *et al.* [2015] identified three types of eddy shapes in the SCS: (i) the bowl-shaped, (ii) the lens-shaped and (iii) the cone-shaped with the largest eddy size at the sea surface, middle depth and eddy bottom, respectively (Figure 5.6). This classification scheme of 3D eddy shape followed the one used by Dong *et al.* [2012] at the Southern California Bight. According to their statistics for eddies in the upper 700 m, about 80% of the total eddies belong to the bowl-shaped group, implying that most eddies in the SCS are surface intensified. Lin *et al.* [2015] mentioned a couple of mechanisms responsible for the generation of the three types of eddies. The bowl-shaped eddies were likely generated by flow instabilities in the upper layer or surface wind stress curl; the lens-shaped eddies were asserted to be generated by flow-shelf slope interactions; and the cone-shaped eddies were generated by current instabilities in the bottom boundary layer. Different mechanisms have also been proposed by other studies for the generation of mesoscale eddies whose cores (or the area where the potential vorticity reaches its maximum) are located at different vertical levels. For example, McGillicuddy [2015] suggested that eddy–wind interaction can locally generate the middle-intensified lenses in the thermocline. Lin *et al.* [2017] also reported an observation of a lens-shaped structure in the SCS and proposed different mechanisms for its generation (detailed in Section 5.3.4).

5.3.4 *Lens-shaped structures*

Subsurface lens-shaped structures have been widely documented in the world's oceans [Kostianoy and Belkin, 1989], termed as intrathermocline eddies [Dugan *et al*., 1982] or submesoscale coherent vortices [McWilliams, 1985]. They are characterized by weak stratification, subsurface velocity maximum, low potential vorticity, etc. [Thomas, 2008]. Most such structures are believed to be generated remotely because they typically have properties different from the ambient waters. Thus, subsurface lens-shaped structures could be potentially important in terms of global transport of mass, heat and salt.

Thermocline lens-shaped structures have been observed in many regions, for example the Japan/East Sea [Gordon *et al*., 2002], the Indian Ocean [Nauw *et al*., 2006], the Pacific coast of the North America [Pelland *et al*., 2013]. They have also been documented in the SCS [Zhang *et al*., 2014b] and the Luzon Strait [Xie *et al*., 2011], but located in the intermediate layer beneath the thermocline. Lens-shaped structures within thermocline, however, had not been observed in the SCS until the report by Lin *et al.* [2017].

Based on *in situ* hydrographic measurements in September 2007, Lin *et al.* [2017] reported on a thermocline lens-shaped structure off the coast of Vietnam in the southwestern SCS. This structure is peculiar in terms of its abnormally large size: the horizontal extent is larger than 220 km (Figure 5.7), much larger than similar structures documented in previous studies. Similar to other intrathermocline lens-shaped structures, this lens also has distinct properties compared to the ambient waters: it is characterized by relatively high temperature, low salinity and low potential vorticity. In order to investigate the generation mechanisms of the observed lens-shaped structure, the authors used a couple of datasets including the ocean reanalysis products provided by the Copernicus Marine Environment Monitoring Service (CMEMS) and the Simple Ocean Data Assimilation (SODA) [Carton and Giese, 2008], satellite-based wind, sea surface temperature (SST) and sea level data. According to the evolution of the thermohaline properties and an analysis of potential vorticity flux, the authors proposed that the observed lens-shaped structure was likely generated by a mixture of two origins: (i) local mixed-layer water and (ii) the water from the coastal jet separation site.

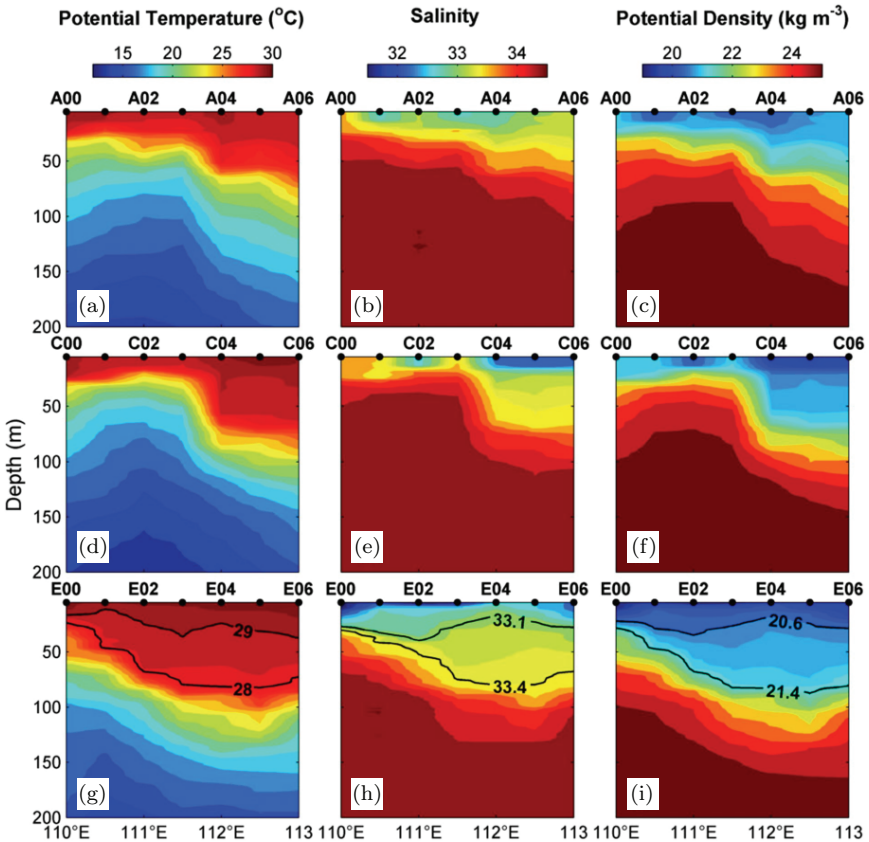

Fig. 5.7. Sectional distributions of thermohaline properties. Potential temperature, salinity and potential density are shown in the left, middle and right columns of panels, respectively. The top, middle and bottom rows of panels are for transects along 13°N, 12°N and 11°N, respectively. The lens-shaped structure is seen in the bottom panels.

Source: Taken from Lin *et al.* [2017].

5.4 Environmental Responses to Mesoscale Eddies in the SCS

Mesoscale eddies have particular characteristics in the horizontal and in the vertical directions as mentioned above, but their influences on the surrounding environment might be, in a way, of more interest/importance. This section will focus on responses of the local thermohaline and circulation,

turbulent mixing, atmosphere and biogeochemical processes to mesoscale eddies in the SCS.

5.4.1 *Thermohaline and circulation responses*

Due to the presence of mesoscale eddies, the local fields of temperature, salinity and velocities are clearly modified. The influences are readily discernible from sea surface to the depths, as already mentioned in Section 5.3 [e.g., Hu *et al*., 2011; Zhang *et al*., 2016]. Nevertheless, the quantitative influence of mesoscale eddies on the regional hydrography still needs to be addressed. Based on five pressure-recording inverted echo sounders (PIES) along a cross-slope section (aligned with a satellite altimetry track) in the northern SCS, Zhao *et al.* [2017] investigated the impact of monsoon winds and mesoscale eddies on the thermohaline structures and circulation patterns. They found that the thermohaline and circulation variability were dominated by a seasonal mode and an eddy mode according to a principal component analysis. The eddy mode, characterized by the passage of mesoscale eddies, accounted for 63% of the total velocity variance and hence significantly affected the local circulation pattern. According to the PIES observations, eddies can affect the distributions of temperature, salinity and velocity down to 860, 150 and 920 m, respectively; and the eddy-induced anomalies of temperature, salinity and velocity can reach up to -2.5°C to 2.2°C, -0.13 to 0.27 psu and -0.4 to 0.38 m s^{-1}, respectively.

Based on a combination of satellite altimeter data, *in situ* measurements and Argo profiles, Chen *et al.* [2012] estimated the eddy heat and salt transports in the SCS within mesoscale eddy fields as well as the entire basin. The so-called eddy transport in mesoscale eddy field is in fact the turbulent transport; the meridional eddy transports of heat and salt are calculated by $\rho C_p v' T'$ and $\rho / S_0 v' S'$, respectively, with ρ the sea water density, C_p the specific heat capacity, S_0 the reference salinity, v', T' and S' being anomalies of meridional velocity, temperature and salinity, respectively (prime denoting deviations from the corresponding temporal means). Chen *et al.* [2012] first estimated eddy transports induced by two anticyclonic eddies in the northern SCS and indicated that the transports were strongly affected by the asymmetric distributions of temperature and salinity in the horizontal and the depths of thermocline and halocline in the vertical. The meridional eddy heat transports induced by

the two eddies reached -6.910 TW ($1\,\text{TW} = 10^{12}$ W) and -10.103 TW with maximum values located at the thermocline, and the eddy salt transports reached 1.139×10^7 and -5.894×10^6 kg s^{-1} with most of the transports confined to the upper 100 m. The authors then statistically estimated the eddy heat and salt transports in the SCS by using all available Argo profiles that were affected by mesoscale eddies. The statistical results showed that the largest heat transports occurred at approximately 70 m while most salt transports were confined to the upper 100 m, similar to results based on the two eddies case. The authors then demonstrated that both heat and salt transports mainly occurred at the depths of thermocline and halocline, but the halocline was shallower than thermocline in the SCS due to the existence of a barrier layer, leading to larger salt transports in the surface layer accompanied by weaker heat transports.

More recently, Sun *et al.* [2018] also examined the eddy-induced transports in the SCS using satellite altimeter data and Argo profiles. They estimated the changes of temperature, salinity, density and velocities induced separately by cyclonic and anticyclonic eddies, respectively. They have also calculated the eddy-induced freshwater transports, which accounted for approximately 8.5% of annual mean transport across the Luzon Strait.

5.4.2 *Turbulent mixing responses*

In addition to the mesoscale thermohaline and circulation structures, smaller-scale processes also exhibit distinct features within mesoscale eddies. Using available Argo profiles from 2006 to 2012 in the northern SCS, Yang *et al.* [2014] estimated the diapycnal mixing within eddy and non-eddy regimes based on the Gregg–Henyey–Polzin parameterization [Kunze *et al*., 2006]. They found that the diffusivity inside an anticyclonic (cyclonic) eddy was significantly higher (lower) than the ambient values outside an eddy. As the background vorticity could be modified by the presence of mesoscale eddies, Yang *et al.* [2014] further inferred that the warm eddy facilitates the downward propagation of near-inertial wave (NIW) energy due to the reduced effective planetary vorticity ($f_{\text{eff}} = f + \zeta/2$) [Kunze, 1985] and hence expanded waveband; by contrast, the cold eddy inhibits the NIW energy propagation.

The modulation of turbulent mixing by an eddy is in fact not uniform. Based on direct microstructure observations across three anticyclonic eddies in the northern SCS (Figure 5.8), Yang *et al.* [2017] reported that mixed-layer turbulent mixing at eddy peripheries was significantly higher, by a factor of five to seven, than that at eddy centers. The authors attributed the

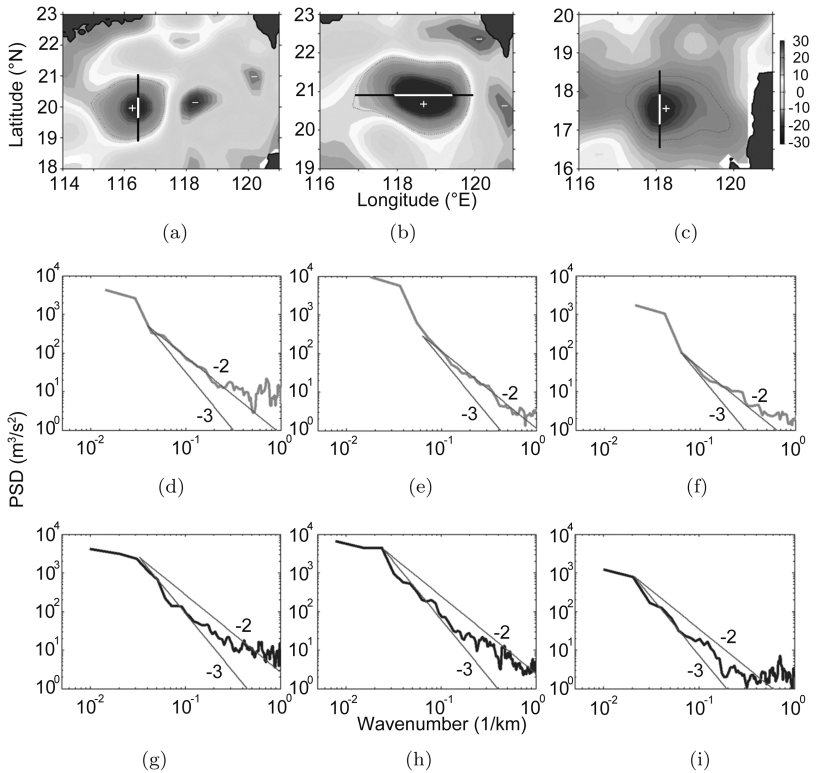

Fig. 5.8. Wavenumber spectra of velocities at eddy periphery and eddy center. (Top) Selected transects across three anticyclonic eddies. Eddy periphery and eddy center are marked with black and white, respectively. Wavenumber spectra of velocities at (middle) eddy periphery and (bottom) eddy center. The cruises were conducted in (left) January 2014, (middle) December 2013 and (right) August 2007. Spectral slopes of k^{-2} and k^{-3} are shown in gray lines. Signs "+" and "−" in the top panels indicate the positive and negative inside, respectively.

Source: Redrawn from Yang *et al.* [2017].

elevated turbulent mixing to enhanced submesoscale motions at the eddy periphery, where the slope of wavenumber spectrum of kinetic energy (k^{-2}) was flatter compared to that at the eddy center (k^{-3}) (Figure 5.8). A forward energy cascade was also found within the submesoscale range (1–10 km) according to the spectral fluxes of kinetic energy at the eddy periphery, while only inverse energy cascade was seen at the same range for spectral fluxes at the eddy center. These findings have profound implications in terms of providing partial evidence that balanced mesoscale motions might transfer energy to smaller scales via generation of submesoscale processes [McWilliams, 2016].

5.4.3 *Atmospheric responses*

Studies of air–sea interactions in the pre-satellite era relied mostly on sparse ship-based observations and coarse-resolution climate models, which only resolved processes at scales larger than a few hundred kilometers [Chelton and Xie, 2010]. Such studies generally indicated a negative correlation between SST and surface wind speed [e.g., Xie, 2004], which was explained as the ocean being passively forced by the atmosphere. However, higher-resolution satellite observations reveal a fundamentally different paradigm of ocean–atmosphere interaction at oceanic mesoscales. A positive correlation between SST and surface wind speed has been globally found at mesoscales, compared to the negative correlation at large scales [Chelton *et al*., 2001, 2007a]. Ocean–atmosphere interactions have also been studied extensively in the SCS based on multiple data sources, including satellite observations [e.g., Xie *et al*., 2003; Wang *et al*., 2012]. Here, we will focus on the impacts of mesoscale eddies on the marine atmospheric boundary layer (the lowest 1–2 km of the atmosphere) in the SCS.

Based on a suite of satellite observations and reanalysis datasets, Xie *et al.* [2003] investigated the seasonal and interannual variations of summertime coastal upwelling off the southern coast of Vietnam and its offshore spread. The authors indicated that the blockage of the southwesterly monsoon by the mountain range (located at the east coast of Vietnam) led to the generation of a strong wind jet which was critical in triggering the coastal upwelling. The coastal cold water was subsequently advected offshore, forming an elongated cold filament, by the northern branch of an anticyclonic eddy developed in summer to the southeast of Vietnam. This anticyclonic eddy was in fact part of a double gyre developed due to intraseasonal changes of the wind through Rossby adjustment [Xie *et al*., 2007]. The authors also showed that the cold filament appeared to reduce the local surface wind speed due to reduced vertical momentum exchange in the marine atmospheric boundary layer. This is a typical example of the two-way ocean–atmosphere interactions in the SCS. Xie *et al.* [2007] further extended the work of Xie *et al.* [2003] showing that the development of the wind jet and offshore cold filament consisted of several intraseasonal events each year with a time interval of approximately 45 d.

More recently, Liu *et al.* [2018] examined the direct atmospheric responses to mesoscale eddies in the SCS. A positive SST-surface wind speed correlation was also found within mesoscale eddy fields in the SCS,

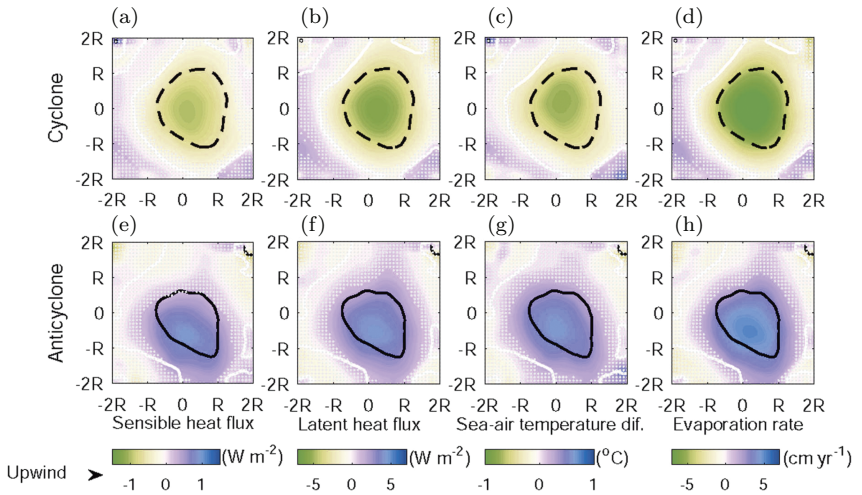

Fig. 5.9. Composite maps of the mean SST anomaly (contours; solid and dashed black lines denote positive and negative values, the white contour being 0°C) superimposed with anomalies of (a), (e) sensible heat flux (color; positive upward), (b), (f) latent heat flux (color; positive upward), (c), (g) sea–air temperature difference (color) and (d), (h) evaporation rate (color) for (upper) cyclonic and (lower) anticyclonic eddies.

Source: Redrawn from Liu *et al.* [2018].

consistent with previous findings in other regions [e.g., Chelton *et al*., 2001, 2007a]. Composite analyses based on 438 eddies suggested that mesoscale eddies affected changes in the overlying turbulent heat fluxes, surface wind speed and evaporation rate by more than 5% of their total variances (Figure 5.9). Mesoscale eddies also influenced changes in the local columnar water vapor, cloud liquid water and rain rate. The authors conducted a numerical simulation to study the dynamical mechanisms and indicated that the local positive correlation between SST and surface wind speed within eddy fields was associated with changes in the atmospheric boundary layer stability caused by eddy-induced heat flux anomalies. By contrast, changes in wind speed at the edges of eddies are associated with the atmospheric pressure gradient forces and atmospheric horizontal advection terms.

5.4.4 *Biogeochemical responses*

In addition to the physical influences, mesoscale eddies also have prominent impacts on regional biogeochemical processes. For a more

comprehensive review of physical–biological–biogeochemical interactions at the ocean mesoscale, the reader is referred to McGillicuddy [2016] who summarized the recent theoretical, observational and numerical progresses in eddy impacts on, for example, upper-ocean chlorophyll, mean properties and fluxes, biological Reynolds stresses, etc. In terms of the biogeochemical responses to mesoscale eddies in the SCS, most of the studies have emerged over the past decade.

A large proportion of physical–biogeochemical coupling studies in the SCS are based on sparse measurements from limited cruises. However, certain consensuses have been achieved among these observational studies. For example, Ning *et al.* [2004] identified higher (lower) concentrations of nutrients, dissolved oxygen, chlorophyll and primary production within cyclonic (anticyclonic) eddies based on summertime and wintertime cruises implemented in the SCS. Enhanced primary production has also been reported by Chen *et al.* [2007] within a cold-core cyclonic eddy sampled around the Luzon Strait, by Hu *et al.* [2014] within various cyclonic eddies sampled in the SCS basin, and by Wang *et al.* [2016] within a cyclonic eddy sampled off the coast of Vietnam. Based on a combination of satellite observations, drifter data and *in situ* measurements, Huang *et al.* [2010] found that the phytoplankton chlorophyll *a* biomass was similar between two anticyclonic eddies and a reference area, but the phytoplankton communities were significantly different in the two eddies because of their different origins and ages. More recently, Wang *et al.* [2018] also reported on similar phytoplankton total chlorophyll *a* among three coherent anticyclonic eddies observed in the SCS [Nan *et al*., 2011b], however, they found significantly elevated biomass at eddy peripheries. Notably, Zhou *et al.* [2013] observed enhanced particle export within an anticyclonic eddy and highlighted the importance of submesoscale processes in the advection from eddy periphery to the core area (Figure 5.10).

Other observational means have also been used in the study of biogeochemical response to mesoscale eddies in the SCS, including satellite, mooring, etc. Lin *et al.* [2010] observed a phytoplankton bloom at a typically oligotrophic site, i.e., the center of the northern SCS. Using a suite of different satellite products and a numerical tracer experiment, the authors concluded that the bloom was associated with an anticyclonic eddy which advected coastal nutrients from the Vietnam coast to the open ocean. He *et al.* [2016] studied the eddy-induced anomalies of surface chlorophyll in the northern SCS using products from multiple satellites. They found that both eddy pumping and eddy stirring were responsible for the

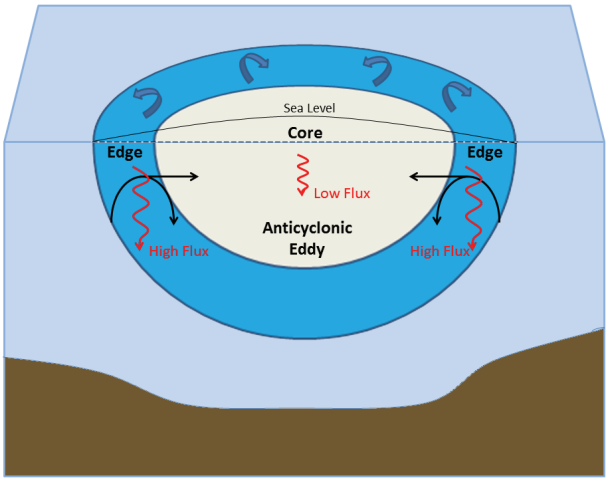

Fig. 5.10. Conceptual scheme of the biogeochemical responses coupled to physical dynamics within an anticyclonic eddy.

Source: Redrawn from Zhou *et al.* [2013].

redistribution of surface chlorophyll. Based on a full-water column mooring system mounted at the depth of 2100 m, Zhang *et al.* [2014a] investigated the deep-sea sediment transport induced by two mesoscale eddies in the northern SCS, and interpreted that the suspended sediments originated from the southwest of Taiwan, trapped by the eddies and transported to the mooring site which was approximately 400 km away from the asserted origin.

In addition to observations, numerical model is obviously another useful tool in studying the physical–biogeochemical interactions associated with mesoscale eddies. As one of the earliest modeling works on the SCS, Xiu and Chai [2011] statistically investigated the roles of mesoscale eddies in redistributing the biological productivity and export flux in the SCS based on a coupled physical–biogeochemical model for the period 1993–2007. They found enhanced (reduced) biogeochemical properties (e.g., chlorophyll, new production, silicate uptake, etc.) in cyclonic (anticyclonic) eddies in the upper 125 m, similar to the findings of Ning *et al.* [2004] based on limited observations. This model has later been used to study the physical and biological controls on the summertime chlorophyll bloom off the coast of Vietnam [Chen *et al.*, 2014]. It has also been applied to investigate the biogeochemical cycles and surface chlorophyll associated with mesoscale

eddies in the SCS [Guo *et al*., 2015, 2017], and similar results were found as in Xiu and Chai [2011].

5.5 Summary

Mesoscale eddies are ubiquitous in the SCS and have been demonstrated to play an important role in local thermodynamics and biogeochemistry. Focusing on studies in the post-altimetry era, this chapter reviews the progress in three main aspects of mesoscale eddies in the SCS: horizontal statistical features, vertical structures and the dynamical impacts.

Horizontal distribution of mesoscale eddies revealed from altimetry suggests that eddies could be generated in almost any place of the SCS deep basin, although several high eddy occurrence areas are found in the southwest of Taiwan, west of Luzon and southeast coast of Vietnam. Existing studies show qualitative agreements on certain statistical eddy properties such as the relatively short eddy lifetime (typically shorter than 60 d), relatively small size (averaged radius of about 100 km) and westward propagation tendency in the SCS. The shorter lifespan and smaller size compared to mesoscale eddies in the open ocean (e.g., Pacific) are due in large to the confinement of solid boundaries in this marginal sea. Considerable discrepancies exist in the detected annual eddy numbers, primarily because of the different eddy identification methods and criteria being used.

The vertical structures of mesoscale eddies in the SCS were overviewed via several prominent examples. Overall, although eddies are typically surface intensified with intensity decreasing with depth, they are capable of influencing the thermohaline structures and velocities in the interior. Mesoscale eddies are often heterogeneous, particularly in their 3D velocity structures. Interestingly, the vertical axis of eddy centers appears to tilt southwestward with increasing depth as reported in two observational studies. Dynamical mechanisms for such a tilt are worthy of further exploration. The 3D eddy detection based on numerical simulations shows that there are also middle- and even bottom-intensified eddies in addition to the most common surface-intensified eddies. In particular, an observed middle-intensified, lens-shaped eddy-like structure was focused on with the potential generation mechanisms being discussed.

In addition to the horizontal and vertical features, the eddy-induced impacts on the local physical and biogeochemical environments were also reviewed. Quantitative estimates suggest that the thermohaline and circulation variability are significantly affected by the passage of mesoscale

eddies. The eddy heat and salt transports occur primarily at the depth of thermocline and halocline, but the largest heat and salt transports are not colocated given the existence of a barrier layer. The ocean–atmosphere interactions within oceanic mesoscale eddies suggest a positive SST-surface wind speed correlation in the SCS, although two-way coupling of the interaction is also seen to the southeast of Vietnam in summer. The biogeochemical responses to mesoscale eddies in the SCS generally reveal higher (lower) tracer concentrations within cyclonic (anticyclonic) eddies. In recent years, submesoscale processes at the peripheries of mesoscale eddies have drawn increasing attention to their impacts on the regional biogeochemistry.

Mesoscale eddies are still a hot topic in the present physical and biogeochemical studies on the SCS. In future, increasing efforts might be shifting from mesoscale to submesoscale, given the enhanced capability in observations and numerical modeling. Several outstanding issues related to mesoscale eddies might be worth exploring further, including for example (i) energy sinks of mesoscale eddies, (ii) roles of submesoscale processes in the evolution of mesoscale eddies and their overall function in the oceanic energy cascade, (iii) 3D distribution and evolution of the biogeochemical tracers in mesoscale eddies and (iv) interdisciplinary collaborations on quantifying eddy-induced material transports or particle fluxes, etc.

Acknowledgments

This study is jointly supported by the National Basic Research Program of China (2015CB954004), the National Natural Science Foundation of China (91958203, 41606009, 41776027 and U1405233), and Laboratory for Regional Oceanography and Numerical Modeling, Pilot National Laboratory for Marine Science and Technology (Qingdao) (No. 2017A02).

References

Carton, J. A. and Giese, B. S. (2008). A reanalysis of ocean climate using Simple Ocean Data Assimilation (SODA), *Mon. Weather Rev.*, 136, pp. 2999–3017.

Chaigneau, A., Gizolme, A. and Grados, C. (2008). Mesoscale eddies off Peru in altimeter records: Identification algorithms and eddy spatiotemporal patterns, *Prog. Oceanogr.*, 79 (2–4), pp. 106–119, doi:10.1016/j.pocean.2008.10.013.

Chelton, D. B. and Xie, S.-P. (2010). Coupled ocean-atmosphere interaction at oceanic mesoscales, *Oceanography*, 23 (4), pp. 52–69.

Chelton, D. B., Esbensen, S. K., Schlax, M. G., Thum, N. and Freilich, M. H. (2001). Observations of coupling between surface wind stress and sea surface temperature in the eastern Tropical Pacific, *J. Clim.*, 14, pp. 1479–1498.

Chelton, D. B., Schlax, M. G. and Samelson, R. M. (2007a). Summertime coupling between sea surface temperature and wind stress in the Californi Current System, *J. Phys. Oceanogr.*, 37, pp. 495–517.

Chelton, D. B., Schlax, M. G., Samelson, R. M. and de Szoeke, R. A. (2007b). Global observations of large oceanic eddies, *Geophys. Res. Lett.*, 34, L15606, doi:10.1029/2007GL 030812.

Chelton, D. B., Schlax, M. G. and Samelson, R. M. (2011). Global observations of nonlinear mesoscale eddies, *Prog. Oceanogr.*, 91 (2), pp. 167–216.

Chen, G., Gan, J., Xie, Q., Chu, X., Wang, D. and Hou, Y. (2012). Eddy heat and salt transports in the South China Sea and their seasonal modulations, *J. Geophys. Res.*, 117, C05021, doi:10.1029/2011JC007724.

Chen, G., Hou, Y., Chu, X. and Hu, P. (2009). The variability of eddy kinetic energy in the South China Sea deduced from satellite altimeter data, *Chin. J. Oceanol. Limnol.*, 27 (4), pp. 943–954.

Chen, G., Hou, Y. and Chu, X. (2011). Mesoscale eddies in the South China Sea: Mean properties, spatiotemporal variability, and impact on thermohaline structure, *J. Geophys. Res.*, 116, C06018, doi:10.1029/2010JC006716.

Chen, G., Xiu, P. and Chai, F. (2014). Physical and biological controls on the summer chlorophyll bloom to the east of Vietnam, *J. Oceanogr.*, 70 (3), pp. 323–328.

Chen, Y.-L. L., Chen, H.-Y., Lin, I.-I., Lee, M.-A. and Chang, J. (2007). Effects of cold eddy on phytoplankton production and assemblages in Luzon Strait bordering the South China Sea, *J. Oceanogr.*, 63, pp. 671–683.

Cheng, X. and Qi, Y. (2010). Variations of eddy kinetic energy in the South China Sea, *J. Oceanogr.*, 66, pp. 85–94.

Cheng, X.-H., Qi, Y.-Q. and Wang, W.-Q. (2005). Seasonal and interannual variabilities of mesoscale eddies in South China Sea (in Chinese with English abstract), *J. Trop. Oceanogr.*, 24 (4), pp. 51–59.

Chu, X., Dong, C. and Qi, Y. (2017). The influence of ENSO on an oceanic eddy pair in the South China Sea, *J. Geophys. Res. Oceans*, 122, pp. 1643–1652, doi:10.1002/ 2016JC012642.

Dale, W. L. (1956). Winds and drift currents in the South China Sea, *Malay. Trop. Geogr.*, 8, pp. 1–31.

Dong, C. M., Lin, X. Y., Liu, Y., Nencioli, F., Chao, Y., Guan, Y., Chen, D., Dickey, T. and McWilliams, J. C. (2012). Three-dimensional oceanic eddy analysis in the Southern California Bight from a numerical product, *J. Geophys. Res. Oceans*, 117, C00H14, doi:10.1029/2011JC007354.

Dugan, J. P., Mied, R., Mignerey, P. and Schuetz, A. F. (1982). Compact, intrathermocline eddies in the Sargasso Sea, *J. Geophys. Res.*, 87, pp. 385–393.

Ferrari, R. and Wunsch, C. (2009). Ocean circulation kinetic energy: Reservoirs, sources, and sinks, *Annu. Rev. Fluid Mech.*, 41, pp. 253–282.

Gan, J. and Qu, T. D. (2008). Coastal jet separation and associated flow variability in the southwest South China Sea, *Deep Sea Res., Part I*, 55, pp. 1–19, doi:10.1016/ j.dsr.2007.09.008.

Gordon, A. L., Giulivi, C. F., Lee, C. M., Furey, H. H., Bower, A. and Talley, L. (2002). Japan/East Sea intrathermocline eddies, *J. Phys. Oceanogr.*, 32, pp. 1960–1974.

Guo, M., Chai, F., Xiu, P., Li, S. and Rao, S. (2015). Impacts of mesoscale eddies in the South China Sea on biogeochemical cycles, *Ocean Dyn.*, 65, pp. 1335–1352, doi:10.1007/ s10236-015-0867-1.

Guo, M., Xiu, P., Li, S., Chai, F., Xue, H., Zhou, K. and Dai, M. (2017). Seasonal variability and mechanisms regulating chlorophyll distribution in mesoscale eddies in the South China Sea, *J. Geophys. Res. Oceans*, 122, pp. 5329–5347, doi:10.1002/2016JC012670.

He, Q., Zhan, H., Cai, S. and Li, Z. (2016). Eddy effects on surface chlorophyll in the northern South China Sea: Mechanism investigation and temporal variability analysis, *Deep Sea Res., Part I*, 112, pp. 25–36.

Hu, J., Gan, J., Sun, Z., Zhu, J. and Dai, M. (2011). Observed three-dimensional structure of a cold eddy in the southwestern South China Sea, *J. Geophys. Res.*, 116, C05016, doi:10.1029/2010JC006810.

Hu, Z., Tan, Y., Song, X., Zhou, L., Lian, X., Huang, L. and He, Y. (2014). Influence of mesoscale eddies on primary production in the South China Sea during spring inter-monsoon period, *Acta Oceanol. Sin.*, 33 (3), pp. 118–128.

Huang, B., Hu, J., Xu, H., Cao, Z. and Wang, D. (2010). Phytoplankton community at warm eddies in the northern South China Sea in winter 2003/2004, *Deep Sea Res., Part II*, 57, pp. 1792–1798.

Hwang, C. and Chen, S.-A. (2000). Circulations and eddies over the South China Sea derived from TOPEX/Poseidon altimetry, *J. Geophys. Res.*, 105 (C10), pp. 23943–23965.

Iselin, C. and Fuglister, F. (1948). Some recent developments in the study of the Gulf Stream, *J. Mar. Res.*, 7 (3), pp. 317–329.

Kostianoy, A. G. and Belkin, I. M. (1989). A survey of observations on intrathermocline eddies in the World Ocean, in J. C. J. Nihoul and B. M. Jamart (Eds.), *Mesoscale/Synoptic Coherent Structures in Geophysical Turbulence*, Elsevier, pp. 821–841.

Kunze, E. (1985). Near-inertial wave propagation in geostrophic shear, *J. Phys. Oceanogr.*, 15 (5), pp. 544–565.

Kunze, E., Firing, E., Hummon, J. M., Chereskin, T. K. and Thurnherr, A. M. (2006). Global abyssal mixing inferred from lowered ADCP shear and CTD strain profiles, *J. Phys. Oceanogr.*, 36 (8), pp. 1553–1576.

Li, L., Nowlin, W. D. and Su, J. (1998). Anticyclonic rings from the Kuroshio in the South China Sea, *Deep Sea Res., Part I*, 45, pp. 1469–1482.

Lin, H., Hu, J. and Zheng, Q. (2012). Satellite altimeter data analysis of the South China Sea and the northwest Pacific Ocean: Statistical features of oceanic mesoscale eddies (in Chinese with English abstract), *J. Oceanogr. Taiwan St.*, 31 (1), pp. 105–113.

Lin, H., Hu, J., Liu, Z., Belkin, I. M., Sun, Z. and Zhu, J. (2017). A peculiar lens-shaped structure observed in the South China Sea, *Sci. Rep.*, 7, 478, doi:10.1038/s41598-017-00593-y.

Lin, I.-I., Lien, C.-C., Wu, C.-R., Wang, G. T. F., Huang, C.-W. and Chiang, T.-L. (2010). Enhanced primary production in the oligotrophic South China Sea by eddy injection in spring, *Geophys. Res. Lett*., 37, L16602, doi:10.1029/2010GL043872.

Lin, P., Wang, F., Chen, Y. and Tang, X. (2007). Temporal and spatial variation characteristics on eddies in the South China Sea, Part I: Statistical analyses (in Chinese with English abstract), *Acta Oceanol. Sin*., 29 (3), pp. 14–22.

Lin, X., Dong, C., Chen, D., Liu, Y., Yang, J., Zou, B. and Guan, Y. (2015). Three-dimensional properties of mesoscale eddies in the South China Sea based on eddy-resolving model output, *Deep Sea Res., Part I*, 99, pp. 46–64.

Liu, H., Li, W., Chen, S., Fang, R. and Li, Z. (2018). Atmospheric response to mesoscale ocean eddies over the South China Sea, *Adv. Atmos. Sci*., 35 (9), pp. 1189–1204, https://doi.org/10.1007/s00376-018-7175-x.

McGillicuddy, D. J. (2015). Formation of intrathermocline lenses by eddy–wind interaction, *J. Phys. Oceanogr*., 45 (2), pp. 606–612.

McGillicuddy, D. J. (2016). Mechanisms of physical-biological-biogeochemical interaction at the oceanic mesoscale, *Annu. Rev. Mar. Sci*., 8, pp. 125–59.

McWilliams, J. C. (1985). Submesoscale, coherent vorticies in the ocean, *Rev. Geophys*., 23, pp. 165–182.

McWilliams, J. C. (2016). Submesoscale currents in the ocean, *Proc. R. Soc. A*, 472, 20160117, doi:10.1098/rspa.2016.0117.

Morrow, R., Birol, F., Griffin, D. and Sudre, J. (2004). Divergent pathways of cyclonic and anticyclonic ocean eddies, *Geophys. Res. Lett*., 31, L24311, doi:10.1029/2004 GL020974.

Nan, F., He, Z., Zhou, H. and Wang, D. (2011b). Three long-lived anticyclonic eddies in the northern South China Sea, *J. Geophys. Res*., 116, C05002, doi:10.1029/2010JC006790.

Nan, F., Xue, H., Xiu, P., Chai, F., Shi, M. and Guo, P. (2011a). Oceanic eddy formation and propagation southwest of Taiwan, *J. Geophys. Res*., 116, C12045, doi:10.1029/2011JC007386.

Nauw, J., van Aken, H., Lutjeharms, J. and de Ruijter, W. P. M. (2006). Intrathermocline eddies in the southern Indian Ocean, *J. Geophys. Res*., 111, C3, doi:10.1029/2005JC002917.

Nencioli, F., Dong, C., Dickey, T. D., Washburn, L. and McWilliams, J. C. (2010). A vector geometry-based eddy detection algorithm and its application to a high resolution numerical model product and high-frequency radar surface velocities in the Southern California Bight, *J. Atmos. Ocean. Technol*., 27 (3), pp. 564–579.

Ning, X., Chai, F., Xue, H., Cai, Y., Liu, C. and Shi, J. (2004). Physical-biological oceanographic coupling influencing phytoplankton and primary production in the South China Sea, *J. Geophys. Res*., 109, C10005, doi:10.1029/2004JC002365.

Okubo, A. (1970). Horizontal dispersion of floatable particles in the vicinity of velocity singularity such as convergences, *Deep Sea Res*., 17, pp. 445–454.

Pelland, N. A., Eriksen, C. C. and Lee, C. M. (2013). Subthermocline eddies over the Washington continental slope as observed by Seagliders, 2003–2009, *J. Phys. Oceanogr.*, 43, pp. 2025–2053.

Qu, T. (2000). Upper-layer circulation in the South China Sea, *J. Phys. Oceanogr.*, 30, pp. 1450–1460.

Sadarjoen, I. A. and Post, F. (2000). Detection, quantification, and tracking of vortices using streamline geometry, *Comput. Graphics*, 24 (3), pp. 333–341, doi:10.1016/S0097-8493(00)00029-7.

Sun, W., Dong, C., Tan, W., Liu, Y., He, Y. and Wang, J. (2018). Vertical structure anomalies of oceanic eddies and eddy-induced transports in the South China Sea, *Remote Sens.*, 10, 795, doi:10.3390/rs10050795.

Thomas, L. N. (2008). Formation of intrathermocline eddies at ocean fronts by wind-driven destruction of potential vorticity, *Dyn. Atmos. Oceans*, 45, pp. 252–273.

Tuo, P., Yu, J.-Y. and Hu, J. (2019). The changing influences of ENSO and the Pacific meridional mode on mesoscale eddies in the South China Sea, *J. Clim.*, 32, pp. 685–700.

Wang, G., Chen, D. and Su, J. (2006). Generation and life cycle of the dipole in the South China Sea summer circulation, *J. Geophys. Res.*, 111, C06002, doi: 10.1029/2005JC003314.

Wang, G., Li, J., Wang, C. and Yan, Y. (2012). Interactions among the winter monsoon, ocean eddy and ocean thermal front in the South China Sea, *J. Geophys. Res.*, 117, C08002, doi:10.1029/2012JC008007.

Wang, G., Su, J. and Chu, P. C. (2003). Mesoscale eddies in the South China Sea observed with altimeter data, *Geophys. Res. Lett.*, 30 (21), 2121, doi:10.1029/2003GL018532.

Wang, J. and Chern, C.-S. (1987a). The warm-core eddy in the northern South China Sea, Part I: Preliminary observations on the warm-core eddy (in Chinese with English abstract), *Acta Oceanogr. Taiwanica*, 18, pp. 92–103.

Wang, J. and Chern, C.-S. (1987b). The warm-core eddy in the northern South China Sea, Part II: A simple mechanism for the establishment and development of the warm-core eddy (in Chinese with English abstract), *Acta Oceanogr. Taiwanica*, 18, pp. 104–113.

Wang, J. and Chern, C.-S. (1997). On the trajectory of subsurface and intermediate waters in the northeastern South China Sea (in Chinese with English abstract), *Trop. Oceanol.*, 16 (2), pp. 24–41.

Wang, L. and Gan, J. (2014). Delving into three-dimensional structure of the West Luzon eddy in a regional ocean model, *Deep Sea Res., Part I*, 90, pp. 48–61.

Wang, L., Huang, B., Laws, E. A., Zhou, K., Liu, X., Xie, Y. and Dai, M. (2018). Anticyclonic eddy edge effects on phytoplankton communities and particle export in the northern South China Sea, *J. Geophys. Res. Oceans*, 123 (11), pp. 7632–7650, doi:10.1029/2017JC013623.

Wang, L., Huang, B., Chiang, K.-P., Liu, X., Chen, B., Xie, Y., Xu, Y., Hu, J. and Dai, M. (2016). Physical-biological coupling in the western South Chin Sea: The

response of phytoplankton community to a mesoscale cyclonic eddy, *PLoS ONE* 11 (4), e0153735, doi:10.1371/journal.pone. 0153735.

Weiss, J. (1991). The dynamics of enstrophy transfer in two dimensional hydrodynamics, *Physica D*, 48, pp. 273–294, doi:10.1016/0167-2789(91)90088-Q.

Xie, L., Tian, J., Zhang, S., Zhang, Y. and Yang, Q. (2011). An anticyclonic eddy in the intermediate layer of the Luzon Strait in Autumn 2005, *J. Oceanogr*., 67, pp. 37–46.

Xie, S.-P. (2004). Satellite observations of cool ocean-atmosphere interaction, *B. Am. Meteorol. Soc*., 85, pp. 195–208.

Xie, S.-P., Chang, C.-H., Xie, Q. and Wang, D. (2007). Intraseasonal variability in the summer South China Sea: Wind jet, cold filament, and recirculations, *J. Geophys. Res*., 112, C10008, doi:10.1029/2007JC004238.

Xie, S.-P., Xie, Q., Wang, D. and Liu, W. T. (2003). Summer upwelling in the South China Sea and its role in regional climate variations, *J. Geophys. Res*., 108, C8, 3261, doi:10.1029/2003JC001867.

Xiu, P. and Chai, F. (2011). Modeled biogeochemical responses to mesoscale eddies in the South China Sea, *J. Geophys. Res*., 116, C10006, doi:10.1029/2010 JC006800.

Xiu, P., Chai, F., Shi, L., Xue, H. and Chao, Y. (2010). A census of eddy activities in the South China Sea during 1993–2007, *J. Geophys. Res*., 115, C03012, doi:10.1029/2009JC005657.

Xu, X., Qiu, Z. and Chen, H. (1982). The general description of the horizontal circulation in the South China Sea (in Chinese with English abstract). *Proceedings of the Symposium of the Chinese Society of Marine Hydrology and Meteorology, Chinese Society of Oceanology and Limnology*, Science Press, Beijing, pp. 137–145.

Yang, H. and Liu, Q. (2003). Forced Rossby wave in the northern South China Sea, *Deep Sea Res., Part I*, 50 (7), pp. 917–926.

Yang, Q., Zhao, W., Liang, X., Dong, J. and Tian, J. (2017). Elevated mixing in the periphery of mesoscale eddies in the South China Sea, *J. Phys. Oceanogr*., 47, pp. 895–907.

Yang, Q., Zhou, L., Tian, J. and Zhao, W. (2014). The roles of Kuroshio intrusion and mesoscale eddy in upper mixing in the northern South China Sea, *J. Coastal Res*., 30, pp. 192–198.

Zhao, R., Zhu, X.-H. and Guo, X. (2017). The impact of monsoon winds and mesoscale eddies on thermohaline structures and circulation patterns in the northern South China Sea, *Cont. Shelf Res*., 143, pp. 240–256.

Zhang, Y., Liu, Z., Zhao, Y., Wang, W., Li, J. and Xu, J. (2014a). Mesoscale eddies transport deep-sea sediments, *Sci. Rep*., 4, 5937, doi:10.1038/srep05937.

Zhang, Z., Qiao, F. and Guo, J. (2014b). Subsurface eddies in the southern South China Sea detected from *in situ* observation in October 2011, *Deep Sea Res., Part I*, 87, pp. 30–34.

Zhang, Z., Tian, J., Qiu, B., Zhao, W., Chang, P., Wu, D. and Wan, X. (2016). Observed 3D structure, generation, and dissipation of oceanic mesoscale eddies in the South China Sea, *Sci. Rep*., 6, 24349, doi:10.1038/srep24349.

Zhang, Z., Zhao, W., Tian, J. and Liang, X. (2013). A mesoscale eddy pair southwest of Taiwan and its influence on deep circulation, *J. Geophys. Res. Oceans*, 118, pp. 6479–6494, doi:10.1002/2013JC008994.

Zheng, Q.-A., Xie, L.-L., Zheng, Z.-W. and Hu, J. (2017). Progress in research of mesoscale eddies in the South China Sea (in Chinese with English abstract), *Adv. Mar. Sci*., 35 (2), pp. 131–158.

Zhou, K., Dai, M., Kao, S.-J., Wang, L., Xiu, P., Chai, F., Tian, J. and Liu, Y. (2013). Apparent enhancement of 234Th-based particle export associated with anti-cyclonic eddies, *Earth Planet. Sci. Lett.*, 381, pp. 198–209.